

# Accurate Direct Positioning in Distributed MIMO Using Delay-Doppler Channel Measurements

Benjamin Deutschmann<sup>1</sup>, Christian Nelson<sup>2</sup>, Mikael Henriksson<sup>3</sup>, Gian Marti<sup>4</sup>,  
Alva Kosasih<sup>5</sup>, Nuutti Tervo<sup>6</sup>, Erik Leitinger<sup>1</sup>, and Fredrik Tufvesson<sup>2</sup>

<sup>1</sup>TU Graz, <sup>2</sup>Lund University, <sup>3</sup>Linköping University, <sup>4</sup>ETH Zurich, <sup>5</sup>KTH Royal Institute of Technology, <sup>6</sup>University of Oulu  
email: benjamin.deutschmann@tugraz.at, christian.nelson@eit.lth.se, mikael.henriksson@liu.se, marti@iis.ee.ethz.ch,  
kosasih@kth.se, nuutti.tervo@oulu.fi, erik.leitinger@tugraz.at, fredrik.tufvesson@eit.lth.se

**Abstract**—Distributed multiple-input multiple-output (D-MIMO) is a promising technology for simultaneous communication and positioning. However, phase synchronization between multiple access points in D-MIMO is challenging, which requires methods that function without the need for phase synchronization. We therefore present a method for D-MIMO that performs direct positioning of a moving device based on the delay-Doppler characteristics of the channel state information (CSI). Our method relies on particle-filter-based Bayesian inference with a state-space model. We use recent measurements from a sub-6 GHz D-MIMO OFDM system in an industrial environment to demonstrate centimeter accuracy under partial line-of-sight (LoS) conditions and decimeter accuracy under full non-LoS.

**Index Terms**—D-MIMO, integrated communication and sensing, direct positioning, particle filter, Bayesian state-filtering, wireless positioning

## I. INTRODUCTION

Next-generation wireless systems are envisioned to integrate communications with sensing capabilities such as positioning [1]–[3], and they are expected to employ geographically separated antennas or access points (APs) [4], [5]. Compared to traditional co-located massive multiple-input multiple-output (MIMO) technology, distributed APs provide significantly increased spatial diversity, which improves coverage throughout the service area and enables more accurate positioning [1], [3], [6]. However, in wireless systems with distributed APs, calibration and synchronization cannot be taken for granted [7]. Next-generation integrated communications and positioning therefore require the development of robust algorithms to the limitations of real-world wireless systems.

### A. Contributions

We present a method for direct positioning in D-MIMO communication systems based on delay-Doppler characteristics of OFDM channel measurements. Our method estimates

This work is supported by the Excellence Center at Linköping – Lund in Information Technology (ELLIIT) and has been done in part during the 2023 ELLIIT focus period “6G – forming a better future.” The project has received funding from the Christian Doppler Research Association and the European Union’s Horizon 2020 research and innovation program under grant agreement No 101013425. Emojis by Twitter, Inc. and others are licensed under CC-BY 4.0.

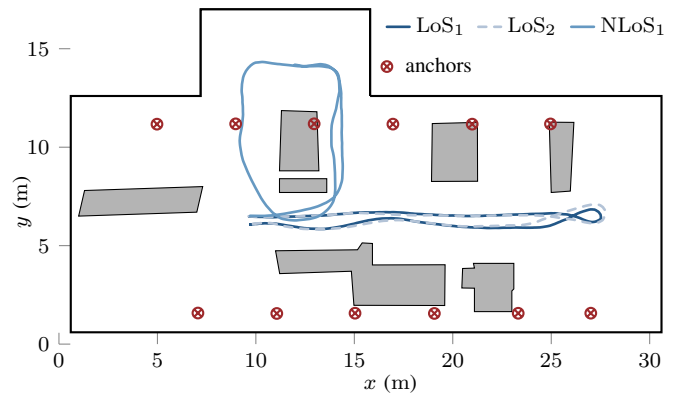


Fig. 1. Floorplan of the industrial hall used for positioning. The floorplan depicts major obstacles (in gray), the twelve distributed receive antennas (in red), and the measured tracks used for positioning (in different shades of blue).

the position of a moving device, called *agent*, through particle-filter-based Bayesian inference in a state-space model where the observations consist of estimates of the channel state information (CSI) between the agent and a set of distributed stationary APs, called *anchors*. No phase synchronization between the anchors is assumed. We evaluate the method on recent measurements of a sub-6 GHz OFDM system [8] between the moving agent and 12 distributed single-antenna anchors that are located in a 30 m × 12 m industrial environment, see Fig. 1. Despite limited bandwidth and no phase synchronization, the results show that our method achieves centimeter-level accuracy under partial line-of-sight (LoS) conditions, and decimeter-accuracy under full non-LoS (NLoS) conditions.

### B. Related Work

The potential of (D-)MIMO CSI for integrated positioning and communications has long been recognized. Reference [9] performs positioning based on Doppler shifts in co-located MIMO. References [10] and [11] perform positioning in D-MIMO based on angle-of-arrival (AoA), but require phase synchronization between the anchors, which may not be available in many practical systems.

An alternative strategy to CSI-based positioning is machine learning-based fingerprinting [12], [13]. However, such an

approach depends on labeled data, which requires expensive measurement campaigns for every deployment.

Phase synchronization, as well as deployment-specific measurement campaigns, can be avoided by estimating the position based on delay-Doppler characteristics [14]. Delay-Doppler-based positioning is used, for example, in global navigation satellite systems (GNSS), where the conventional strategy is a two-step approach that first estimates delays and radial velocities, and then maps these estimates to the position domain [15]. However, it has been shown [16], [17] that a direct approach, where the position is estimated directly from the receive signal rather than from intermediary delay and velocity estimates, is more robust. References [18] and [19] have also combined direct delay-Doppler tracking based on particle filters, similar to ours. However, since the focus of these works is not on simultaneous positioning and communications, their position estimates are formed based on specialized positioning signals. In contrast, our method is based on CSI estimates of conventional OFDM systems. Moreover, these other works evaluate their methods through simulations that do not contain scattering or blockage, which may be unsuited for integrated positioning and communication scenarios. In contrast, we show the efficacy of our method on measured data from a real-world environment that contains both scattering and blockage.

*Notation:* Column vectors and matrices are denoted by boldface lowercase (e.g.,  $\mathbf{x}$ ) and uppercase letters (e.g.,  $\mathbf{X}$ ), respectively. We use  $\mathbf{x}^\top$  and  $\mathbf{x}^H$  to denote the transpose and Hermitian transpose of  $\mathbf{x}$ , respectively. The Euclidean norm of  $\mathbf{x}$  is  $\|\mathbf{x}\|$ . The  $N \times N$  identity matrix is  $\mathbf{I}$ , where the size is left implicit. The operator  $\text{vec} : \mathbb{C}^{M \times N} \rightarrow \mathbb{C}^{MN} : \mathbf{X} \mapsto \mathbf{x}$  vectorizes the matrix  $\mathbf{X}$  by stacking its columns on top of each other. We use  $\exp(\mathbf{x})$  to denote the vector obtained by applying the exponential function to each entry of  $\mathbf{x}$ .

## II. MEASUREMENT SCENARIO

The measurements used for positioning were done in an industrial environment at the Department of Mechanical Engineering Sciences at Lund University (see Fig. 2) with a channel sounder developed at Lund University [8]. The sounder is designed for D-MIMO and implements an orthogonal frequency-division multiplexing (OFDM) sounding principle. The carrier frequency was set to  $f_c = 3.75$  GHz, with  $N_f = 449$  subcarriers spaced 78.125 kHz apart, resulting in a measurement bandwidth of  $B = 35$  MHz. All radio units were disciplined with an external 10 MHz clock and a 1 pulse per second (1PPS) signal for frequency synchronization, but they were not calibrated on site and were lacking phase synchronization. The post-calibrations performed are detailed in [8].

Serving as anchors,  $M = 12$  single dipole antennas were distributed along the long sides of the industrial hall, see Fig. 1 and 2. To maximize coverage at floor level and to mitigate the strong reflection of the walls behind them, the antennas were tilted  $45^\circ$  downward relative to the wall.

Serving as the agent, a remote-controlled robot with a single antenna at 1 m height was driving through the environment



Fig. 2. Photo of the positioning environment. The industrial hall is approximately 30 m long and 12 m wide, with a ceiling height varying between 8 m and 12 m depending on position.

with a maximum speed of 1 m/s. The agent transmits pilots every  $\Delta t = 5$  ms resulting in 200 channel estimates per second.

In this paper we focus on the representative scenarios shown in Fig. 1. In LoS<sub>1</sub>, the agent moves through the middle aisle of the industrial hall and back. There are multiple anchor links under LoS conditions throughout the track, but many anchors are blocked by machinery through significant portions. We refer to the conditions of LoS<sub>1</sub> as “partial LoS.” Track LoS<sub>2</sub> is approximately identical to LoS<sub>1</sub> but was recorded at a later time for control purposes. In NLoS<sub>1</sub>, the agent moves in circles around a piece of machinery such that there are parts of the trajectory where all anchor links are under NLoS conditions. We therefore refer to the conditions of NLoS<sub>1</sub> as “full NLoS.”

## III. SYSTEM MODEL

### A. Channel Model

We assume that at each sample index  $k \in \{1, \dots, K\}$  (corresponding to sample times  $t_k \in \{t_1, \dots, t_K\}$  with  $\Delta t \triangleq t_{k+1} - t_k$ ), every anchor  $m \in \{1, \dots, M\}$  obtains a noisy estimate of the channel between itself and the moving agent

$$\tilde{\mathbf{h}}_k^{(m)} = \mathbf{h}_k^{(m)} + \mathbf{n}_k^{(m)}. \quad (1)$$

Here,  $\tilde{\mathbf{h}}_k^{(m)} \in \mathbb{C}^{N_f}$  is the estimate of the frequency-domain channel vector  $\mathbf{h}_k^{(m)} \in \mathbb{C}^{N_f}$  with carrier frequency  $f_c$  and baseband frequencies  $\mathbf{f} \in \mathbb{R}^{N_f}$ , and  $\mathbf{n}_k^{(m)}$  is observation noise which we model as white Gaussian noise,  $\mathbf{n}_k^{(m)} \sim \mathcal{CN}(\mathbf{0}, \sigma^2 \mathbf{I})$ . For simplicity, we do not explicitly model scattering and blockage due to the machinery and large amount of metal surfaces in the environment (see Fig. 2). Instead, we model the channels as pure line-of-sight (LoS) links. We assume that the channel amplitudes stay approximately constant for  $N_t$  subsequent samples. We denote the unknown position and (purely planar) velocity of the moving agent at time index  $k$  by  $\mathbf{p}_k \in \mathbb{R}^3$  and  $\mathbf{v}_k = [v_k^{(x)}, v_k^{(y)}, v_k^{(z)}]^\top \in \mathbb{R}^2 \times \{0\}$ , respectively, and we assume that these quantities remain approximately constant for  $N_t$  subsequent samples. The position of the  $m$ th anchor is denoted by  $\mathbf{p}^{(m)} \in \mathbb{R}^3$ , and is assumed to be known.

These assumptions allow us to model  $N_t$  subsequent noise-free channel vectors  $\mathbf{H}_k^{(m)} = [\mathbf{h}_{k-N_t+1}^{(m)}, \dots, \mathbf{h}_k^{(m)}] \in \mathbb{C}^{N_f \times N_t}$  as<sup>1</sup>

$$\mathbf{H}_k^{(m)} = \alpha_k^{(m)} \mathbf{b}_k^{(m)} \mathbf{c}_k^{(m)\top}, \quad (2)$$

where  $\alpha_k^{(m)} \in \mathbb{C}$  is the complex channel amplitude between the moving agent and the  $m$ th anchor at sample index  $k$ ,  $\mathbf{b}_k^{(m)} \in \mathbb{C}^{N_f}$  is the temporal response vector, and  $\mathbf{c}_k^{(m)} \in \mathbb{C}^{N_t}$  is the Doppler response vector.

The Doppler response vector  $\mathbf{c}_k^{(m)}$  captures how the channel phases evolves during the time frame  $\mathbf{t} = [t_{k-N_t+1}, \dots, t_k]^\top$  due to the moving agent's velocity  $\mathbf{v}_k$ , and can be written as

$$\mathbf{c}_k^{(m)} = \exp\left(j2\pi \frac{f_c}{c} \left\langle \frac{\mathbf{p}^{(m)} - \mathbf{p}_k}{\|\mathbf{p}^{(m)} - \mathbf{p}_k\|}, \mathbf{v}_k \right\rangle \mathbf{t}\right), \quad (3)$$

where  $c$  is the speed of light, and where the inner product represents the radial velocity of the moving agent into the direction of the  $m$ th anchor. The temporal response vector  $\mathbf{b}_k^{(m)}$  in (2) accounts for the different phase shifts at the different frequencies  $\mathbf{f}$  due to the propagation delay  $c^{-1}\|\mathbf{p}^{(m)} - \mathbf{p}_k\|$ , and can be expressed as

$$\mathbf{b}_k^{(m)} = \exp\left(-j2\pi \frac{\|\mathbf{p}^{(m)} - \mathbf{p}_k\|}{c} \mathbf{f}\right). \quad (4)$$

Finally, the complex amplitude  $\alpha_k^{(m)}$  in (2) accounts for path loss, the common phase shift at the carrier frequency  $f_c$  due to the propagation delay  $c^{-1}\|\mathbf{p}^{(m)} - \mathbf{p}_k\|$ , as well as phase offset at the  $m$ th anchor due to the absence of phase synchronization.

### B. State-Space Model

Our goal is to estimate the agent trajectory  $\{\mathbf{p}_k\}_{k=1}^K$  based on the observations

$$\mathbf{Y}_k = [\text{vec}(\widetilde{\mathbf{H}}_k^{(1)}), \dots, \text{vec}(\widetilde{\mathbf{H}}_k^{(M)})] \in \mathbb{C}^{N_t N_f \times M}, \quad (5)$$

for  $k = 1, \dots, K - N_t + 1$ , where  $\widetilde{\mathbf{H}}_k^{(m)} = [\widetilde{\mathbf{h}}_{k-N_t+1}^{(m)}, \dots, \widetilde{\mathbf{h}}_k^{(m)}]$  are the noisy observations of  $\mathbf{H}_k^{(m)}$  according to (1). Since the moving agent's positions  $\{\mathbf{p}_k\}_{k=1}^K$  are related to each other via the velocities  $\{\mathbf{v}_k\}_{k=1}^K$ , we perform tracking in a nearly constant velocity state-space model

$$\mathbf{x}_k = \Phi \mathbf{x}_{k-1} + \mathbf{w}_k, \quad (6)$$

where

$$\mathbf{x}_k = [\mathbf{p}_k^\top \ v_k^{(x)} \ v_k^{(y)} \ \sigma^2]^\top \in \mathcal{S}, \quad (7)$$

is the state vector,<sup>2</sup>  $\Phi$  is the transition matrix

$$\Phi = \begin{bmatrix} 1 & 0 & 0 & \Delta t & 0 & 0 \\ 0 & 1 & 0 & 0 & \Delta t & 0 \\ 0 & 0 & 1 & 0 & 0 & 0 \\ 0 & 0 & 0 & 1 & 0 & 0 \\ 0 & 0 & 0 & 0 & 1 & 0 \\ 0 & 0 & 0 & 0 & 0 & 1 \end{bmatrix}, \quad (8)$$

<sup>1</sup>For ease of notation, we assume here that estimates of  $N_t$  channel vectors have already been acquired at time step  $k = 1$ .

<sup>2</sup>Note that the state vector does not represent the vertical agent velocity  $v_k^{(z)}$ , which is identical to zero, nor the complex amplitude  $\alpha_k^{(m)}$ , which we treat as a nuisance parameter, see below. Note also that the channel noise variance  $\sigma^2$  from (1) is modeled as a (constant) variable of interest.

and where  $\mathbf{w}_k \sim \mathcal{N}(\mathbf{0}, \text{diag}(\sigma_p^2, \sigma_p^2, \sigma_{v_x}^2, \sigma_{v_y}^2, \sigma_v^2, \sigma_s^2))$  models process noise. We use  $\mathcal{S} = \mathbb{R}^5 \times \mathbb{R}_{\geq 0}$  to denote the entire state space. The dependency of the observations  $\mathbf{Y}_k$  on the states  $\mathbf{x}_k$  is modelled as follows: We assume the measurements at the anchors to be independent, so the likelihood of  $\mathbf{Y}_k = [\mathbf{y}_k^{(1)}, \dots, \mathbf{y}_k^{(M)}]$  conditional on  $\mathbf{x}_k$  and  $\alpha_k = [\alpha_k^{(1)}, \dots, \alpha_k^{(M)}]^\top$  is

$$p(\mathbf{Y}_k | \mathbf{x}_k, \alpha_k) = \frac{\prod_{m=1}^M \exp\left(-\frac{1}{\sigma^2} \|\mathbf{y}_k^{(m)} - \alpha_k^{(m)} \psi_k^{(m)}\|^2\right)}{(\pi \sigma^2)^{MN_f N_t}}. \quad (9)$$

where  $\psi_k^{(m)} \triangleq \text{vec}(\mathbf{b}_k^{(m)} \mathbf{c}_k^{(m)\top})$  is the *delay-Doppler response*. We treat the unknown amplitudes  $\alpha_k^{(m)}$  as nuisance parameters. Hence, we compute the *profile likelihood*, i.e., we *concentrate* [20] with respect to  $\alpha_k$  by computing maximum likelihood (ML) estimates conditional on  $\mathbf{x}_k$  (since the doppler-Delay response  $\psi_k^{(m)}$  is a function of  $\mathbf{x}_k$ )

$$\hat{\alpha}_k^{(m)} | \mathbf{x}_k = \arg \max_{\alpha_k^{(m)}} p(\mathbf{y}_k^{(m)} | \mathbf{x}_k, \alpha_k^{(m)}) = \frac{\psi_k^{(m)\text{H}} \mathbf{y}_k^{(m)}}{\|\psi_k^{(m)}\|^2}. \quad (10)$$

Reinserting  $\hat{\alpha}_k^{(m)} | \mathbf{x}_k$  in (9), our profile likelihood yields

$$p(\mathbf{Y}_k | \mathbf{x}_k) = \frac{\exp\left(-\frac{1}{\sigma^2} \sum_{m=1}^M \|\Pi_{m,k}^\perp \mathbf{y}_k^{(m)}\|^2\right)}{(\pi \sigma^2)^{MN_f N_t}} \quad (11)$$

where  $\Pi_{m,k}^\perp = \mathbf{I} - \frac{\psi_k^{(m)} \psi_k^{(m)\text{H}}}{\|\psi_k^{(m)}\|^2}$  is the projector onto the orthogonal complement of the subspace spanned by  $\psi_k^{(m)}$ . Note that the profile likelihood in (11) is a function of the agent's position  $\mathbf{p}_k$  and velocity  $\mathbf{v}_k$  since  $\Pi_{m,k}^\perp$  is a function of the delay-Doppler response  $\psi_k^{(m)}$ .

## IV. DELAY-DOPPLER POSITIONING AND TRACKING

### A. Recursive Bayesian Filtering

We formulate the tracking problem through the Bayesian filtering equation [21]

$$p(\mathbf{x}_k | \mathbf{Y}_{1:k}) = \frac{p(\mathbf{Y}_k | \mathbf{x}_k) p(\mathbf{x}_k | \mathbf{Y}_{1:k-1})}{p(\mathbf{Y}_k | \mathbf{Y}_{1:k-1})} \quad (12)$$

that describes the posterior density  $p(\mathbf{x}_k | \mathbf{Y}_{1:k})$  of the state vector  $\mathbf{x}_k$  at time step  $k$  given past observations (i.e., measurements)  $\mathbf{Y}_{1:k-1}$  and the current observation  $\mathbf{Y}_k$ .

The Chapman-Kolmogorov equation relates the prediction density  $p(\mathbf{x}_k | \mathbf{Y}_{1:k-1})$  in (12) to the old posterior  $p(\mathbf{x}_{k-1} | \mathbf{Y}_{1:k-1})$  and the proposal density  $p(\mathbf{x}_k | \mathbf{x}_{k-1}, \mathbf{Y}_{1:k-1})$  which—given the first-order Markovity of our model, see (6) and (9)—equals  $p(\mathbf{x}_k | \mathbf{x}_{k-1})$ , i.e.,  $p(\mathbf{x}_k | \mathbf{x}_{k-1}, \mathbf{Y}_{1:k-1}) = p(\mathbf{x}_k | \mathbf{x}_{k-1})$ . By the Chapman-Kolmogorov equation, we thus have

$$p(\mathbf{x}_k | \mathbf{Y}_{1:k-1}) = \int_{\mathcal{S}} p(\mathbf{x}_k | \mathbf{x}_{k-1}) p(\mathbf{x}_{k-1} | \mathbf{Y}_{1:k-1}) d\mathbf{x}_{k-1}. \quad (13)$$

By the law of total probability, the normalization constant in (12) can be expressed in continuous integral form through

$$p(\mathbf{Y}_k | \mathbf{Y}_{1:k-1}) = \int_{\mathcal{S}} p(\mathbf{Y}_k | \mathbf{x}_k, \mathbf{Y}_{1:k-1}) p(\mathbf{x}_k | \mathbf{Y}_{1:k-1}) d\mathbf{x}_k. \quad (14)$$

## B. Particle-Based Approximation

We implement the recursive Bayesian filter from Sec. IV-A through a particle filter [22] that approximates the posterior distribution with a set of  $N$  particles  $\{\mathbf{x}_k^{(i)}\}_{i=1}^N$  at time step  $k$  with prediction (i.e., prior) weights

$$w_{k|k-1}^{(i)} \propto \mathbb{P}(\mathbf{x}_k = \mathbf{x}_k^{(i)} | \mathbf{Y}_{1:k-1}) \quad (15)$$

that reflect the probability of the state  $\mathbf{x}_k$  represented by the particle  $\mathbf{x}_k^{(i)}$  given the past observations  $\mathbf{Y}_{1:k-1}$ . The prediction density in (13) is approximated by

$$\hat{p}(\mathbf{x}_k | \mathbf{Y}_{1:k-1}) = \sum_{i=1}^N w_{k|k-1}^{(i)} \delta(\mathbf{x}_k - \mathbf{x}_k^{(i)}) \quad (16)$$

which leads to the following approximation of (12):

$$\hat{p}(\mathbf{x}_k | \mathbf{Y}_{1:k}) = \sum_{i=1}^N \underbrace{c_k^{-1} p(\mathbf{Y}_k | \mathbf{x}_k^{(i)}) w_{k|k-1}^{(i)}}_{\triangleq w_{k|k}^{(i)}} \delta(\mathbf{x}_k - \mathbf{x}_k^{(i)}), \quad (17)$$

where  $c_k = \sum_{i=1}^N p(\mathbf{Y}_k | \mathbf{x}_k^{(i)}) w_{k|k-1}^{(i)}$ , which approximates the normalization constant  $p(\mathbf{Y}_k | \mathbf{Y}_{1:k-1})$  in (14), ensures that  $\sum_{i=1}^N w_{k|k}^{(i)} = 1$ .

We estimate the state  $\mathbf{x}_k$  by approximating the minimum mean square error (MMSE) estimate

$$\mathbf{x}_k^{\text{MMSE}} = \mathbb{E}\{\mathbf{x}_k | \mathbf{Y}_{1:k}\} = \int_S \mathbf{x}_k p(\mathbf{x}_k | \mathbf{Y}_{1:k}) d\mathbf{x}_k \quad (18)$$

as

$$\hat{\mathbf{x}}_k = \int_S \mathbf{x}_k \hat{p}(\mathbf{x}_k | \mathbf{Y}_{1:k}) d\mathbf{x}_k = \sum_{i=1}^N \mathbf{x}_k^{(i)} w_{k|k}^{(i)}, \quad (19)$$

and we approximate the corresponding state covariance matrix

$$\mathbf{P}_k^{\text{MMSE}} = \int_S (\mathbf{x}_k - \mathbf{x}_k^{\text{MMSE}}) (\mathbf{x}_k - \mathbf{x}_k^{\text{MMSE}})^\top p(\mathbf{x}_k | \mathbf{Y}_{1:k}) d\mathbf{x}_k$$

as

$$\hat{\mathbf{P}}_k = \sum_{i=1}^N (\mathbf{x}_k^{(i)} - \hat{\mathbf{x}}_k) (\mathbf{x}_k^{(i)} - \hat{\mathbf{x}}_k)^\top w_{k|k}^{(i)}. \quad (20)$$

## C. Particle Filter Implementation

Algorithm 1 summarizes the implemented particle filter. For simplicity, we initialize  $N$  particles by sampling from a Gaussian distribution  $p_{\mathbf{x}_0} = \mathcal{N}(\hat{\mathbf{x}}_0, \hat{\mathbf{P}}_0)$  and assigning weights  $w_{1|0}^{(i)} = 1/N$ . The posterior in (17) is computed by the loop starting at line 3. Although computationally expensive, it is well suited for parallel computing, while the resampling in line 11 is generally not parallelizable. Note that  $w_{k|k-1}^{(i)} = w_{k-1|k-1}^{(i)}$  on line 5 comes from the choice of using the state-space model as the proposal density. We choose a regularized particle filter [23] using a Gaussian kernel with an implementation similar to [22, Alg. 6]. That is, in each step  $k$ , we evaluate (20) and decompose  $\hat{\mathbf{P}}_k = \mathbf{L}_k \mathbf{L}_k^\top$  using the Cholesky decomposition. In line 11, we employ systematic resampling [22, Alg. 2] which reduces particle degeneracy, and implies equal weights after resampling (see line 12). After resampling, each particle is convolved (see line 16) with a regularization Gaussian kernel  $K(\mathbf{x}_k)$  with covariance matrix

## Algorithm 1: Regularized Particle Filter

---

**Input :**  $N, \hat{\mathbf{x}}_0, \hat{\mathbf{P}}_0, \{\mathbf{Y}_k\}_{k=1}^K$   
**Output:**  $\{\hat{\mathbf{x}}_k\}_{k=1}^K$

- 1  $\mathbf{x}_1^{(i)} \sim p_{\mathbf{x}_0}$  and  $w_{1|1}^{(i)} \leftarrow 1/N \forall i \in \{1 \dots N\}$ ;
- 2 **for**  $k \leftarrow 1$  **to**  $K$  **by** 1 **do**
- 3     **for**  $i \leftarrow 1$  **to**  $N$  **by** 1 **do**
- 4          $\mathbf{x}_k^{(i)} \leftarrow \Phi \mathbf{x}_{k-1}^{(i)} + \mathbf{w}_k^{(i)}$ ;     //see (6)
- 5          $w_{k|k-1}^{(i)} \leftarrow w_{k-1|k-1}^{(i)}$ ;
- 6          $\tilde{w}_{k|k}^{(i)} \leftarrow p(\mathbf{Y}_k | \mathbf{x}_k^{(i)}) w_{k|k-1}^{(i)}$ ;     //see (11)
- 7     **end**
- 8      $\{w_{k|k}^{(i)}\}_{i=1}^N \leftarrow \{\tilde{w}_{k|k}^{(i)} / (\sum_{i=1}^N \tilde{w}_{k|k}^{(i)})\}_{i=1}^N$ ;
- 9      $\hat{\mathbf{x}}_k \leftarrow \sum_{i=1}^N \mathbf{x}_k^{(i)} w_{k|k}^{(i)}$      //see (19)
- 10     $\hat{\mathbf{P}}_k \leftarrow \sum_{i=1}^N (\mathbf{x}_k^{(i)} - \hat{\mathbf{x}}_k) (\mathbf{x}_k^{(i)} - \hat{\mathbf{x}}_k)^\top w_{k|k}^{(i)}$ ;     //see (20)
- 11     $\mathbf{x}_k^{(i)} \leftarrow \text{resample}(\{\mathbf{x}_k^{(i)}, w_{k|k}^{(i)}\})$ ;     //see [22, Alg. 2]
- 12     $\{w_{k|k}^{(i)}\}_{i=1}^N \leftarrow 1/N$ ;     //due to resampling
- 13     $\mathbf{L}_k \leftarrow \text{cholesky}(\hat{\mathbf{P}}_k)$ ;     //s.t.  $\mathbf{L}_k \mathbf{L}_k^\top = \hat{\mathbf{P}}_k$
- 14    **for**  $i \leftarrow 1$  **to**  $N$  **by** 1 **do**
- 15          $\boldsymbol{\epsilon}_i \sim \mathcal{N}(\mathbf{0}, \mathbf{I})$ ;
- 16          $\mathbf{x}_k^{(i)} \leftarrow \mathbf{x}_k^{(i)} + h_{\text{opt}} \mathbf{L}_k \boldsymbol{\epsilon}_i$ ;
- 17    **end**
- 18 **end**

---

$\hat{\mathbf{P}}_k$  and scaled by the optimal kernel bandwidth  $h_{\text{opt}}$  [23, p. 253] to counteract particle impoverishment.

## V. RESULTS

Algorithm 1 is initialized by drawing  $N = 16'000$  particles from  $p_{\mathbf{x}_0}$  around an (deliberately inaccurate) mean  $\hat{\mathbf{x}}_0 = [6, 9, 1.5]^\top \text{m}$  and is given the channel measurements  $\{\mathbf{Y}_k\}_{k=1}^K$  in each step  $k$ . Fig. 3 shows the estimated trajectories  $\{\hat{\mathbf{x}}_k\}_{k=1}^K$  (—) for each of the tracks LoS<sub>1</sub> (top), LoS<sub>2</sub> (center), and NLoS<sub>1</sub> (bottom) in comparison to the ground truth (—). We use a “large” covariance matrix  $\hat{\mathbf{P}}_0$  for initialization to ensure that particles cover a large portion of the state space, which may result in  $\hat{\mathbf{x}}_k$  being strongly influenced by multiple modes in the posterior distribution at the initial stage of the trajectory (see NLoS<sub>1</sub>). Our temporal window size is chosen as  $N_t = 200$ . For process noise, we intentionally choose a small  $\sigma_p = 0.3 \text{ mm}$  and  $\sigma_h = 2 \text{ cm}$  to promote particles that stay close to the “true” mode (i.e., at  $\mathbf{p}_k$ ) in the posterior distribution, a large  $\sigma_v = 0.1 \text{ m/s}$  to accommodate the largest expected acceleration, and  $\sigma_S = 0.3$ .

In partial LoS, i.e., when at least some anchors (⊙) are visible from the agent, our algorithm achieves centimeter-level accuracy. After convergence, we achieve a planar position root mean square error (RMSE) of 9.4 cm on track LoS<sub>1</sub> and an RMSE of 9.1 cm on track LoS<sub>2</sub>. On the NLoS<sub>1</sub> track, where parts of the track are in complete NLoS, our algorithm achieves an RMSE of 49.9 cm.

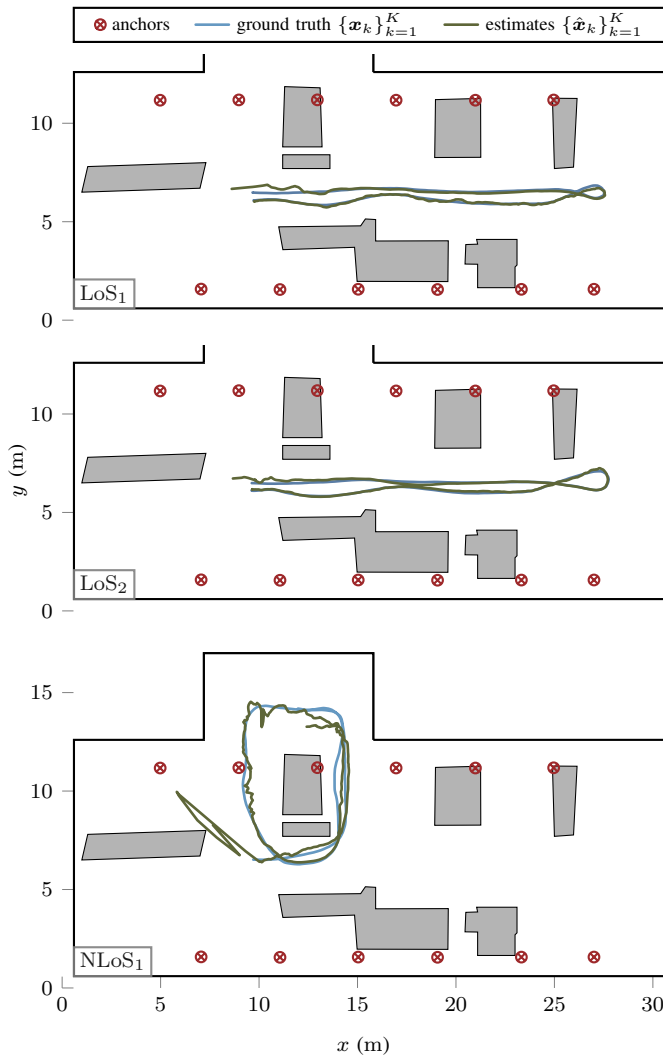


Fig. 3. Estimated trajectories (—) vs. true trajectories (—) for the tracks LoS<sub>1</sub>, LoS<sub>2</sub>, and NLoS<sub>1</sub>.

## VI. CONCLUSIONS

We have shown the possibility of positioning in an industrial environment using a direct positioning-based method on delay-Doppler characteristics. The method is evaluated on real-world D-MIMO measured CSI, which has proper frequency synchronization but lacks phase synchronization. Despite limited bandwidth and a sub-6 GHz carrier, we show centimeter accuracy in partial LoS, and decimeter accuracy in full NLoS.

## REFERENCES

- [1] F. Liu, Y. Cui, C. Masouros, J. Xu, T. X. Han, Y. C. Eldar, and S. Buzzi, "Integrated sensing and communications: Toward dual-functional wireless networks for 6G and beyond," *IEEE J. Sel. Areas Commun.*, vol. 40, no. 6, pp. 1728–1767, Jun. 2022.
- [2] A. Behravan, V. Yajnanarayana, M. F. Keskin, H. Chen, D. Shrestha, T. E. Abrudan, T. Svensson, K. Schindhelm, A. Wolfgang, S. Lindberg, and H. Wymeersch, "Positioning and sensing in 6G: Gaps, challenges,

and opportunities," *IEEE Veh. Technol. Mag.*, vol. 18, no. 1, pp. 40–48, Mar. 2023.

- [3] A. Fascista, B. J. B. Deutschmann, M. F. Keskin, T. Wilding, A. Coluccia, K. Witrals, E. Leitinger, G. Seco-Granados, and H. Wymeersch, "Uplink joint positioning and synchronization in cell-free deployments with radio stripes," in *Proc. IEEE Int. Conf. Commun. Workshops (ICC Workshops)*, May 2023, pp. 1330–1336.
- [4] D. Wang, J. Wang, X. You, Y. Wang, M. Chen, and X. Hou, "Spectral efficiency of distributed MIMO systems," *IEEE J. Sel. Areas Commun.*, vol. 31, no. 10, pp. 2112–2127, Oct. 2013.
- [5] E. Nayebi, A. Ashikhmin, T. L. Marzetta, and H. Yang, "Cell-free massive MIMO systems," in *Proc. Asilomar Conf. Signals, Syst. Comput.*, Oct. 2015, pp. 695–699.
- [6] V. Savić and E. G. Larsson, "Fingerprinting-based positioning in distributed massive MIMO systems," in *Proc. IEEE Veh. Technol. Conf.*, Sep. 2015, pp. 1–5.
- [7] E. G. Larsson, "Massive synchrony in distributed antenna systems," *IEEE Trans. Signal Process.*, vol. 72, pp. 855–866, 2024.
- [8] C. Nelson, X. Li, A. Fedorov, B. Deutschmann, and F. Tufvesson, "Distributed MIMO measurements for integrated communication and sensing in an industrial environment," *Sensors*, vol. 24, no. 5, p. 1385, Feb. 2024.
- [9] H. Chen, F. Jiang, Y. Ge, H. Kim, and H. Wymeersch, "Doppler-enabled single-antenna localization and mapping without synchronization," in *Proc. IEEE Global Commun. Conf. (GLOBECOM)*, Dec. 2022, pp. 6469–6474.
- [10] S. Yang, D. Zhang, R. Song, P. Yin, and Y. Chen, "Multiple WiFi access points co-localization through joint AoA estimation," *IEEE Trans. Mobile Comput.*, vol. 23, no. 2, pp. 1488–1502, Feb. 2023.
- [11] A. Blanco, P. J. Mateo, F. Gringoli, and J. Widmer, "Augmenting mmWave localization accuracy through sub-6 GHz on off-the-shelf devices," in *Proc. Int. Conf. Mobile Syst., App. Services*, Jun. 2022, pp. 477–490.
- [12] E. Gönültaş, E. Lei, J. Langerman, H. Huang, and C. Studer, "CSI-based multi-antenna and multi-point indoor positioning using probability fusion," *IEEE Trans. Wireless Commun.*, vol. 21, no. 4, pp. 2162–2176, Apr. 2021.
- [13] S. De Bast, A. P. Guevara, and S. Pollin, "CSI-based positioning in massive MIMO systems using convolutional neural networks," in *Proc. IEEE Veh. Technol. Conf. (VTC)*, 2020, pp. 1–5.
- [14] I. Shames, A. N. Bishop, M. Smith, and B. D. O. Anderson, "Doppler shift target localization," *IEEE Trans. Aerosp. Electron. Syst.*, vol. 49, no. 1, pp. 266–276, Jan. 2013.
- [15] F. Vincent, J. Vilà-Valls, O. Besson, D. Medina, and E. Chaumette, "Doppler-aided positioning in GNSS receivers – a performance analysis," *Signal Proc.*, vol. 176, 2020.
- [16] P. Closas, C. Fernandez-Prades, and J. A. Fernandez-Rubio, "Maximum likelihood estimation of position in GNSS," *IEEE Signal Process. Lett.*, vol. 14, no. 5, pp. 359–362, May 2007.
- [17] P. Closas and A. Gusi-Amigo, "Direct position estimation of GNSS receivers: Analyzing main results, architectures, enhancements, and challenges," *IEEE Signal Process. Mag.*, vol. 34, no. 5, pp. 72–84, Sep. 2017.
- [18] A. Y. Sidi and A. J. Weiss, "Delay and doppler induced direct tracking by particle filter," *IEEE Trans. Aerosp. Electron. Syst.*, vol. 50, no. 1, pp. 559–572, Jan. 2014.
- [19] J.-A. Luo, J. He, and D.-L. Peng, "Towards fast and accurate 3D direct emitter tracking via laplace approximation," *IEEE Trans. Veh. Technol.*, vol. 73, no. 1, pp. 28–44, Jan. 2023.
- [20] P. Stoica and A. Nehorai, "On the concentrated stochastic likelihood function in array signal processing," *Circ., Syst., Signal Proc.*, vol. 14, no. 5, pp. 669–674, Sep. 1995.
- [21] F. Gustafsson, "Particle filter theory and practice with positioning applications," *IEEE Aerosp. Electron. Syst. Mag.*, vol. 25, no. 7, pp. 53–82, Jul. 2010.
- [22] M. Arulampalam, S. Maskell, N. Gordon, and T. Clapp, "A tutorial on particle filters for online nonlinear/non-Gaussian Bayesian tracking," *IEEE Trans. Signal Process.*, vol. 50, no. 2, pp. 174–188, Feb. 2002.
- [23] C. Musso, N. Oudjane, and F. Le Gland, *Sequential Monte Carlo Methods in Practice*. Springer New York, 2001, ch. 12: "Improving regularised particle filters," pp. 247–271.